minerals

MDPI

Article

Mineralogy of Zn–Hg–S and Hg–Se–S Series Minerals in Carbonate-Hosted Mercury Deposits in Western Hunan, South China

Jianping Liu [1,2], Yanan Rong [1] and Shugen Zhang [1,*]

[1] Key Laboratory of Metallogenic Prediction of Nonferrous Metals and Geological Environment Monitoring, Ministry of Education, Central South University, Changsha 410083, China; liujianping@csu.edu.cn (J.L.); rongyn19@163.com (Y.R.)

[2] Key Laboratory of Mineralogy and Metallogeny, Guangzhou Institute of Geochemistry, Chinese Academy of Sciences, Guangzhou 510460, China

* Correspondence: zhangshugenzsg@163.com; Tel.: +86-731-888-30616

Academic Editor: Radostina Atanassova
Received: 10 May 2017; Accepted: 12 June 2017; Published: 15 June 2017

Abstract: Among the Zn–Hg–S and Hg–Se–S series minerals, Hg-bearing sphalerite and metacinnabar are uncommon in ore deposits, but they are useful indicators of temporal variation of ore forming fluids, as well as presenting metallurgical implications for Hg-bearing deposits. To understand the Hg–Zn–Se mineralization system of the Tongren–Fenghuang Hg Belt (TFHB), the Zn–Hg–S and Hg–Se–S series minerals of the Chashula Hg–Zn and Dongping Hg–Ag–Se carbonate-hosted deposits were studied by microscopic observation, electron-probe microanalysis, and X-ray diffraction analysis. Observations show that the Chashula and Dongping deposits experienced two stages of mineralization (Stages 1 and 2). The pyrite, sphalerite I (Hg-poor sphalerite), and quartz formed in Stage 1, while the Zn-bearing cinnabar, sphalerite II (Hg-bearing sphalerite), cinnabar, selenium metacinnabar, and Ag minerals formed in Stage 2. The Hg-bearing sphalerite, containing 13.36–22.26 wt % Hg (average 18.73 wt % Hg), replaces sphalerite I (0.00–1.31 wt % Hg). The Hg-bearing sphalerite of the Dongping Hg–Ag–Se deposit contains lower Hg (10.12–14.67 wt % Hg) than that of the Chashula deposit. The unit cell *a* of the Hg-bearing sphalerite gradually increases with increasing Hg content. The texture of the Zn-bearing cinnabar shows it is not stable and easily breaks down to Hg-bearing sphalerite and cinnabar through the chemical reaction: (Hg,Zn)S → (Zn,Hg)S + HgS. Selenium metacinnabar intergrowths with tetrahedrite and miargyrite were found only in the Dongping deposit. The selenium metacinnabar contains 76.57–83.97 wt % Hg, and extensive isomorphic substitution of Se and S (6.81–19.21 wt % Se, 4.14–10.32 wt % S). Based on our mineralogical studies, the Zn, Hg, Hg–Zn, and Hg–Se mineralization styles in the TFHB are interpreted as the product of different stages in the mineralization process.

Keywords: Hg-bearing sphalerite; selenium metacinnabar; mineral chemistry; Tongren–Fenghuang Hg Belt; south China

1. Introduction

Dill [1] states, "mercury is exceptional among the elements for its liquid state". The Hg contents of Earth's upper, middle, and lower crust are ~0.05, 0.0079, and 0.014 ppm, respectively [2]. It is widely used in batteries, dental amalgam, lighting, measuring devices, switches and relays, and thermostats [3,4]. Based on the geological setting, there are four types of Hg deposit: (1) magmatic; (2) structure-related; (3) sedimentary [1]; and (4) carbonate-hosted Hg deposits [5,6], of which magmatic Hg deposits provide important Hg ore reserves [1]. Carbonate-hosted Hg deposits as a minor type of

Hg resource, are distributed locally in the Terlingua district in Texas (USA) [5] and in south China [6,7]. However, carbonate-hosted Hg deposits are the most important Hg deposits in China, accounting for 90% of the Hg ore reserves, and they are distributed predominantly in Guizhou, Hunan and Chongqing provinces [6–8].

Although Hg abundance in Earth's crust is low, 90 Hg minerals have been found, including native metals and intermetallic alloys, halides, sulfides, arsenides, selenides, antimonides, tellurides, sulfosalts, oxides, carbonates, and sulfates [9]. More widespread than any other Hg mineral, cinnabar and metacinnabar are the most important Hg ore minerals [1]. Among Hg minerals, the Zn–Hg–S–Se component minerals forming the ZnS (sphalerite)–HgS (metacinnabar) series and the HgS (metacinnabar)–HgSe (tiemannite) series [10] in deposits have attracted more attention because of their significance in terms of ore formation and metallurgical applications, especially Hg-bearing sphalerite [11,12]. Hg-bearing sphalerite in Europe, the Soviet Union, and America was studied in the 1940s to 1960s [13]. Sphalerite containing 8.20 wt % Hg was found in the Oued Maden deposit in Tunisia by Slim-Shimi and Tlig [14] in 1993 [15]. Hg-bearing sphalerite has been found recently in the Eskay Creek volcanogenic massive sulfide deposit (British Columbia, Canada) containing 0.08–16.35 wt % Hg [11], and in the Rujevavac vein polymetallic deposit in Serbia containing 0.30–6.47 wt % Hg [12]. Tiemannite is probably the most common Se mineral, with widespread occurrences reported in Hg deposits [16]. However, there is little information about Hg–Zn–Se–S minerals in carbonate-hosted Hg deposits.

The Tongren–Fenghuang Hg Belt (TFHB), also called the Xiangqian Hg Belt, in southern China (Figure 1a) hosts many large deposits of carbonate-hosted Hg deposits. Unlike cinnabar, sphalerite and selenium metacinnabar are distributed locally in the TFHB [17–20], and form Hg–Se, Zn–Hg, and Zn orebodies [21–28]. In addition, Hg-bearing sphalerite has also been reported in the TFHB [19,20,29,30]. Although the structural geology and geochemistry of the TFHB have been studied [31–36], there are no studies regarding the conditions of formation that generated the different styles of mineralization in the belt. Although some mineral chemical data on Hg-bearing sphalerite and tiemannite have been obtained, there is no detailed information about the spatial distribution of Hg-bearing sphalerite in these deposits or about Hg isomorphism in the sphalerite during the mineralization processes. Furthermore, there have been no comparative studies of Hg-sphalerite in the different Hg deposits within the TFHB. The Chashula deposit with its distinct Hg, Hg–Zn, and Zn ore zones, and the Dongping Hg–Ag–Se deposit with its abundant selenium metacinnabar provide excellent examples with which to better understand the Hg–Zn–Se mineralization system.

In this paper, the chemical composition and crystal parameters of Hg-sphalerite and associated minerals of the Chashula Hg and the Dongping Hg–Ag deposits are studied, with the aim of characterizing the distribution pattern of Hg-bearing sphalerite and Hg–Zn–S–Se series minerals in the carbonate-hosted Hg deposits.

2. Geological Setting

2.1. Regional Geology of the Tongren–Fenghuang Hg Belt

The TFHB is located in the northeastern part of the Xiangxi (western Hunan)–Qiandong (eastern Guizhou) Pb–Zn–Hg metallogenic belt (Figure 1a), at the southeastern margin of the Yangtze Block [37]. The TFHB hosts many super-large- to large-medium-scale Hg deposits and it accounts for half of the total Hg reserves in China [38]. The TFHB consists mainly of Cambrian to Ordovician carbonate formations, and the Hg deposits occur preferentially in the slope facies of the Cambrian carbonate formations between the Baojing–Tongren Fault and Guzhang–Jishou–Fenghuang Fault (Figure 1b). The TFHB has a SW–NE orientation, and it is 150 km long and 5–10 km wide. The ore belt is divided into three segments from SW to NE: (1) the southern segment consisting of the Xinhuang, Wanshan, and Dachala orefield; (2) the central segment consisting of the Chatian orefield; and (3) the northern segment consisting of the Huoziping orefield and Shuiyingdong orefield [38]. The deposits

are controlled by regional NW-trending faults; they are super-large to large–medium in size in the central and southern segments but small in the northern segment [38]. The orebodies are hosted predominantly in the dolomite of the Middle Cambrian, with a few hosted in the limestone and dolomite of the Lower Cambrian, and they consist of two types: (1) gently inclined conformable types; and (2) steeply inclined vein types. Moreover, the ore minerals and mineralization are also distinctly different in each type. Thus, ore minerals in the southern segment consist mainly of cinnabar without sphalerite and with local stibnite; in the central segment, they consist of cinnabar and sphalerite in widely developed Hg–Zn mineralization ore zones [39]; and, in the northern segment, they consist of cinnabar with tiemannite and Ag minerals.

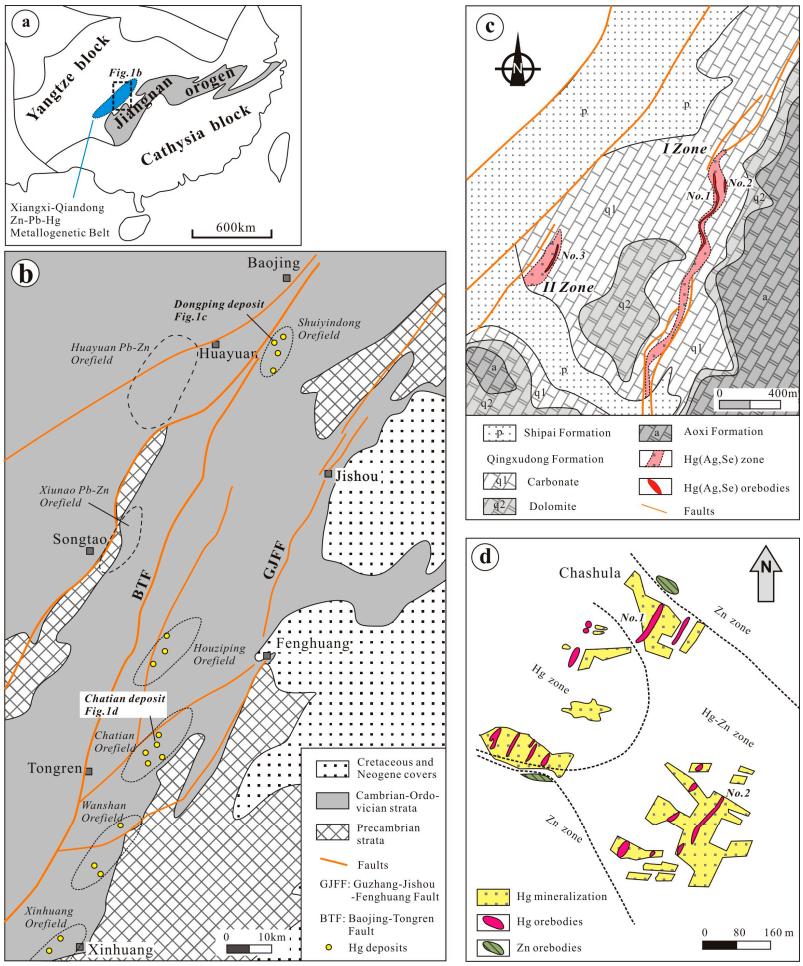

Figure 1. (**a**) Map of the tectonic units in southern China, showing the Xiangxi–Qiandong Pb–Zn–Hg metallogenic belt located in the southeast of the Yangtze Block and the Jiangnan orogen belt; (**b**) simplified geological map of western Hunan–Eastern Guizhou region showing distribution of Hg orefield and adjacent Pb–Zn orefield (after HBGMR, unpublished maps); (**c**) geological map of the Dongping deposit (after [40]); and (**d**) simplified geological map of the Chashula deposit, showing the distribution of Hg, Hg–Zn, and Zn mineralization zones (after [41]).

2.2. Geology of the Studied Deposits

2.2.1. The Chashula Hg–Zn Deposit

The Chashula deposit is located in the central part of the Chatian orefield [39]. The deposit was explored in the 1960s, and a total metal reserve of 465 t Hg with an average grade of 0.37% Hg was obtained by the No. 405 Geology Team of the Hunan Bureau of Geology and Mineral Resources

(HBGMR). The orebodies are strata-bounded in the lamellar dolomite of the Middle Cambrian. Six lenticular orebodies (including the two largest: No. 1 and 2, Figure 1d) were delineated with lengths, widths, and average thicknesses of 130–500, 40–200, and 0.54–3.98 m, respectively. Based on the ore types and mineral assemblages, the deposit can be divided into three ore zones; namely a central Hg zone, followed outwards by an Hg–Zn zone, and then Zn zone (Figure 1d; [28,41]). The Hg zone is composed of cinnabar without sphalerite; the Zn–Hg zone is composed of cinnabar and sphalerite, while the Zn zone is composed by sphalerite and negligible cinnabar. The Hg-rich orebodies are located in the Hg zone, which is related to brecciation. From our investigation, the three types of ore have distinct characteristics (Figure 2a–c); the Hg ores are breccia-type ores with cinnabar (Figure 2a), while the Hg–Zn and Zn ores are irregular vein type ores (Figure 2b,c). The Hg–Zn ore is composed of light-colored sphalerite with cinnabar and metacinnabar (Figure 2b), while the Zn ores contain sphalerite only (Figure 2c).

2.2.2. The Dongping Hg–Ag–Se Deposit

The Dongping deposit is located in the northwest of the Shuiyingdong orefield (Figure 1b). The deposit was explored in the 1990s, and 110 t Ag with an average grade of 100.8 g/t Ag, 3185 t Hg with an average grade of 0.12–0.17 wt % Hg, and 267 t Se with an average grade of 0.01 wt % Se were obtained by the No. 405 Geological Team in 1994 [40]. Two ore zones (No. I and II) are hosted by faults zones occurring in the carbonates of the Lower Cambrian Qingxudong Formation. The NNE-trending No. I ore zone (Figure 1c) is 1650 m long and 15–70 m wide, while the NE-trending No. II is 400 m long and 25–110 m wide. Three main orebodies, named No. 1 Hg–Ag–Se orebody, No. 2, and No. 3 Hg orebodies (Figure 1c) have been outlined. The orebodies have a lenticular form, SE orientation with a dip of 20°–45°, length of 150–500 m, down dip of 100 m, and thickness of 1.27–1.53 m [40]. The Hg–Ag–Se ores are vein type bodies and they composed mainly of selenium metacinnabar (Figure 2d).

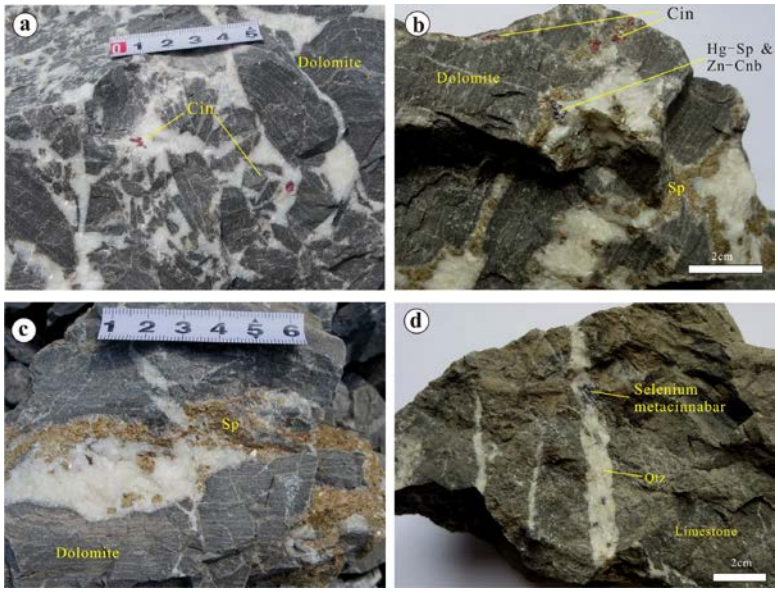

Figure 2. Photographs of typical mineralization style: (**a**) brecciated Hg ores, located in Hg zone of the Chashula deposit, showing dolomite breccia, dolomite cements, and disseminated cinnabar; (**b**) Hg–Zn ores located in Hg–Zn zone of the Chashula deposit, showing cinnabar, sphalerite, Hg-bearing sphalerite, and Zn-bearing cinnabar in irregular vein filling in dolomite; (**c**) Zn ores, located in the Zn zone of the Chashula deposit, showing sphalerite only in irregular vein-filling in dolomite; and (**d**) Hg–Ag ores of the No. I zone at the Dongping deposit, containing selenium metacinnabar, miargyrite, Hg-bearing freibergite in quartz (Qtz) vein filling in limestone.

3. Sampling and Analytical Methods

3.1. Sampling Site

Samples were collected from abandoned ore stockpiles. The Hg–Zn and Zn ore samples were located in the Hg–Zn and Zn mineralization zones of the Chashula deposit, respectively. The Hg–Ag ore samples were collected from the No. 1 Hg–Ag–Se orebodies of the Dongping deposit.

3.2. Electron-Probe Microanalyses

Ore minerals and ore textures were observed in polished sections using standard reflected-light microscopy techniques. The chemical compositions of the minerals were analyzed by electron probe microanalysis (EPMA) using a Shimadzu EPMA-1720H housed at the School of Geosciences and Info-physics (SGI), Central South University (CSU), Changsha, China. The operating conditions of the electron microprobe were maintained at an accelerating voltage of 15 kV, beam current of 10 nA, and an electron beam diameter of 1 μm. The X-ray lines used to analyze the different elements were as follows: S$K\alpha$, Fe$K\alpha$, Zn$K\alpha$, Se$L\alpha$, Cd$L\alpha$, and Hg$M\alpha$. Mineral and metal standards used for calibration of elemental X-ray intensities included pyrite (Fe), sphalerite (S and Zn), bismuth selenide (Se), greenockite (Cd), and cinnabar (Hg). The resulting data were then ZAF corrected using proprietary Shimadzu software.

3.3. X-ray Diffraction Analysis

The X-ray diffraction (XRD) analysis was performed directly on polished sections with an X-ray microbeam using a Rigaku D/Max Rapid IIR microdiffractometer at 40 kV and 250 mA, using a Cu tube and a 0.05-mm collimator with 20-min exposure. A 22° omega angle was used for the analysis. Samples were rotated in the fixed plane during measurements. The raw XRD data were processed with Jade 6.0 software (Materials Data Incorporated, Livermore, CA, USA), displaying a 20 range of 20°–100°. Peaks were matched using ICDD pdf. Unit cell refinements were processed using the cell refinement module of the Jade 6.0 software. The XRD analysis was also performed at the SGI, CSU, China.

4. Results

4.1. Ore Petrology

4.1.1. The Chashula Deposit

Ore minerals of the Chashula deposit are relatively simple, composed mainly of cinnabar and sphalerite with trace pyrite and Zn-bearing cinnabar. All sulfides occur as veinlets or disseminated forms filling quartz and dolomite (Figure 3c). Two generations of pyrite and sphalerite are identified. The first-generation pyrites (pyrite I) are euhedral to subhedral intergrown with first-generation sphalerite (sphalerite I) hosted in quartz (Figure 3a), while the second-generation (pyrite II) are vein filling in cinnabar and sphalerite (Figure 3c,d). The two generations of sphalerite (sphalerite I and II) are distinguished in reflectance, insofar as sphalerite II is lower than sphalerite I. Based on the EPMA data (see Section 4.2) sphalerite II is Hg-bearing sphalerite, which occurs in minor amounts, but it is distributed widely in the Hg–Zn ores. Four types of Hg-bearing sphalerite were observed: (1) as rims around sphalerite (Figure 4a,b); (2) as veins filling in microfractures in sphalerite (Figure 4d); (3) as grains filling in dolomite (Figure 4e,f); and (4) as fine vermicular inclusions in cinnabar enveloping Zn-bearing cinnabar (Figure 4g,h). Sphalerite II is always intergrown with cinnabar in the Hg–Zn ores. Zinc-bearing cinnabar was also found in the Hg–Zn ores, and it is replaced by cinnabar and vermicular Hg-bearing sphalerite inclusions in the cinnabar around the boundary of the Zn-bearing cinnabar (Figure 4a,g,h). Based on the mineral assemblages and crosscutting relationships, two stages of mineralization (Stages 1 and 2) are identified (Figure 5). Quartz, pyrite I, and sphalerite I were

formed in Stage 1, and sphalerite II, Zn-bearing cinnabar, and cinnabar and dolomite were formed in Stage 2.

4.1.2. The Dongping Deposit

The ore minerals of the Hg–Ag–Se ores are composed of selenium metacinnabar, miargyrite, freibergite with small amounts of sphalerite (I and II) and pyrite (Figure 6d–f). Sulfides aggregates fill the intercrystalline interstices of the quartz and calcite grains. Similar to the Hg–Zn ores, two generations of sphalerite were also observed in the Hg–Ag–Se ores. Sphalerite I forms intergrowths with pyrite hosted in quartz (Figure 6a). Sphalerite II is Hg-bearing sphalerite based on the EPMA data (see Section 4.2), and it occurs as island-like inclusions in miargyrite (Figure 6b), replacement remnants in miargyrite (Figure 6b), or inclusions in selenium metacinnabar (Figure. 6c). Selenium metacinnabar occurs interstitially in dolomite, or as sulfide aggregates including miargyrite and Hg-bearing freibergite (Figure 6d–f) in dolomite and quartz. The selenium metacinnabar fills quartz with/without calcite (Figure 6e,f). Based on the crosscutting relationships, two stages of mineralization (Stages 1 and 2) were identified (Figure 7). Stage 1 is similar to Stage 1 in the Chashula deposit, whereas Stage 2 hosts selenium metacinnabar, Hg-bearing freibergite, and miargyrite, which contrasts with the simpler mineral assemblage of Stage 2 in the Chashula deposit.

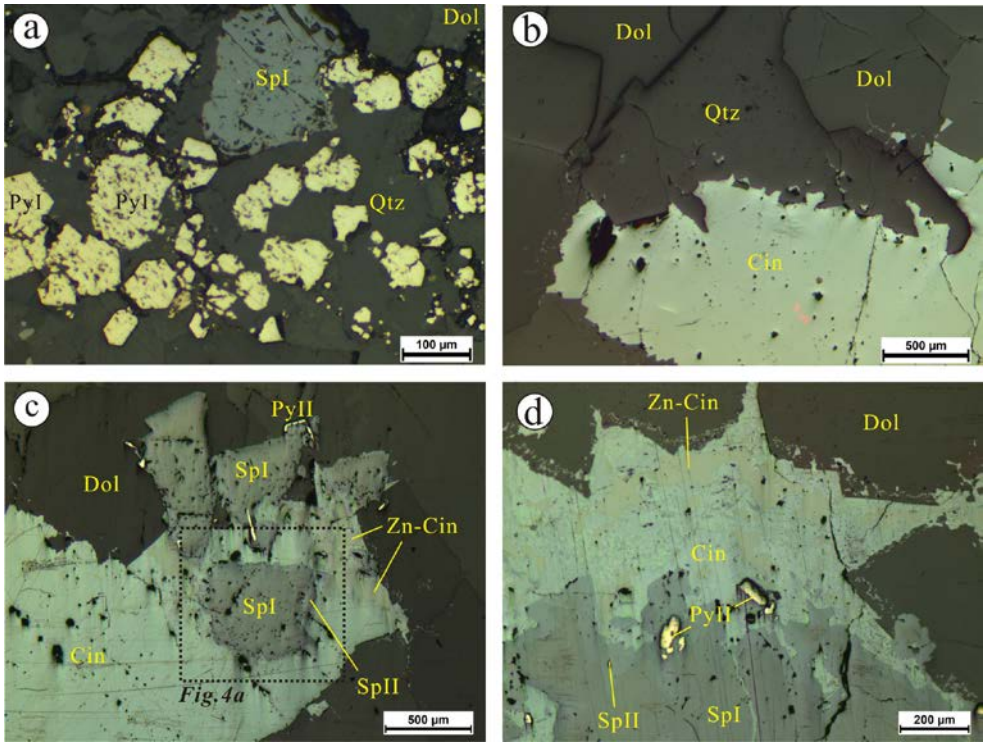

Figure 3. Photomicrographs of ore minerals and textures in the Chashula deposit: (**a**) euhedral to subhedral first-generation pyrite I (PyI) with sphalerite I (SpI) in quartz (Qtz); (**b**) cinnabar (Cin) filling quartz (Qtz) and dolomite (Dol); (**c**) sphalerite I and Zn-bearing cinnabar (Zn-Cin) replaced by cinnabar (Cin); and (**d**) sphalerite I replaced by sphalerite II (SpII), and the Zn-bearing cinnabar (Zn-Cin) replaced by cinnabar (Cin).

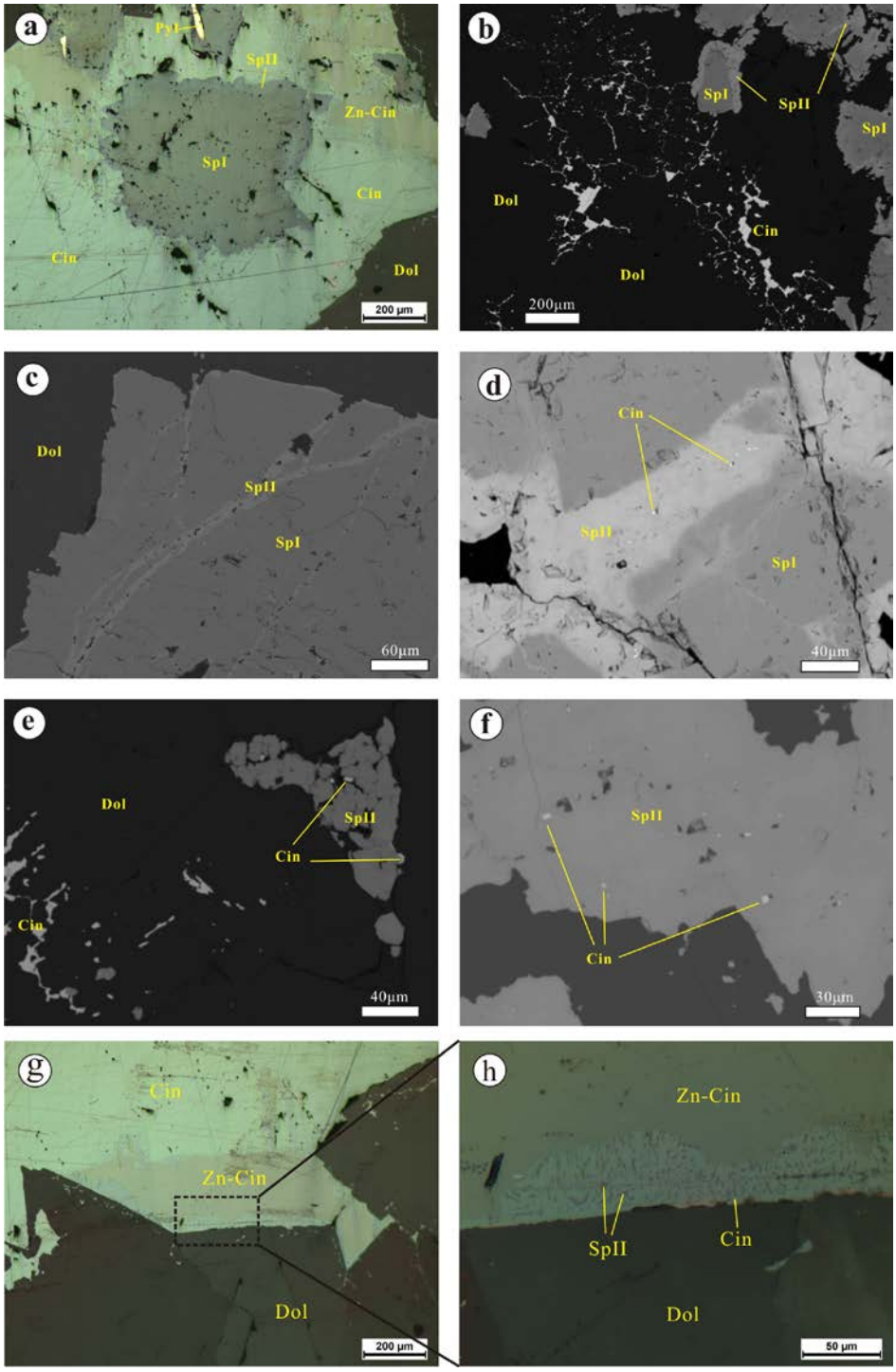

Figure 4. Photomicrographs (**a**,**g**,**h**) and backscattered electron images (**c**–**f**) of sphalerite II (SpII). (**a**) enlargement of Figure 3c with sphalerite II forming a rim around the sphalerite I (SpI), sphalerite I included in cinnabar (Cin), and zinc-bearing cinnabar (Zn-Cin) also replaced by cinnabar; (**b**) sphalerite II replace sphalerite I, and cinnabar forming interstitial network in dolomite; (**c**) sphalerite II replace sphalerite I along the surface and fractures of sphalerite I; (**d**) sphalerite II replace sphalerite I in fracture, and cinnabar present in Hg-bearing sphalerite; (**e**) sphalerite II grains with cinnabar filling dolomite (Dol); (**f**) cinnabar inclusions in sphalerite II; (**g**) Zn-bearing cinnabar (Zn-Cin) replaced by cinnabar (Cin), with vermicular sphalerite II in cinnabar located at replacement boundary; and (**h**) detailed view of Figure 4g, showing vermicular sphalerite II intergrowth in cinnabar.

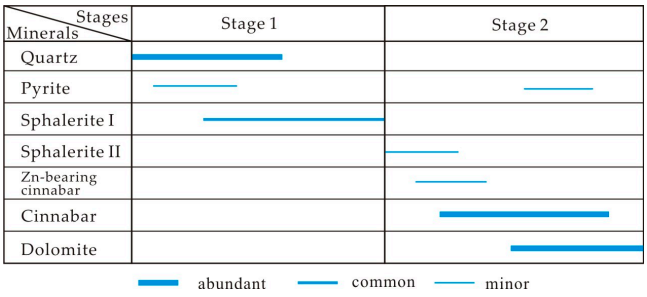

Figure 5. Paragenetic diagram of the Chashula Hg–Zn deposit.

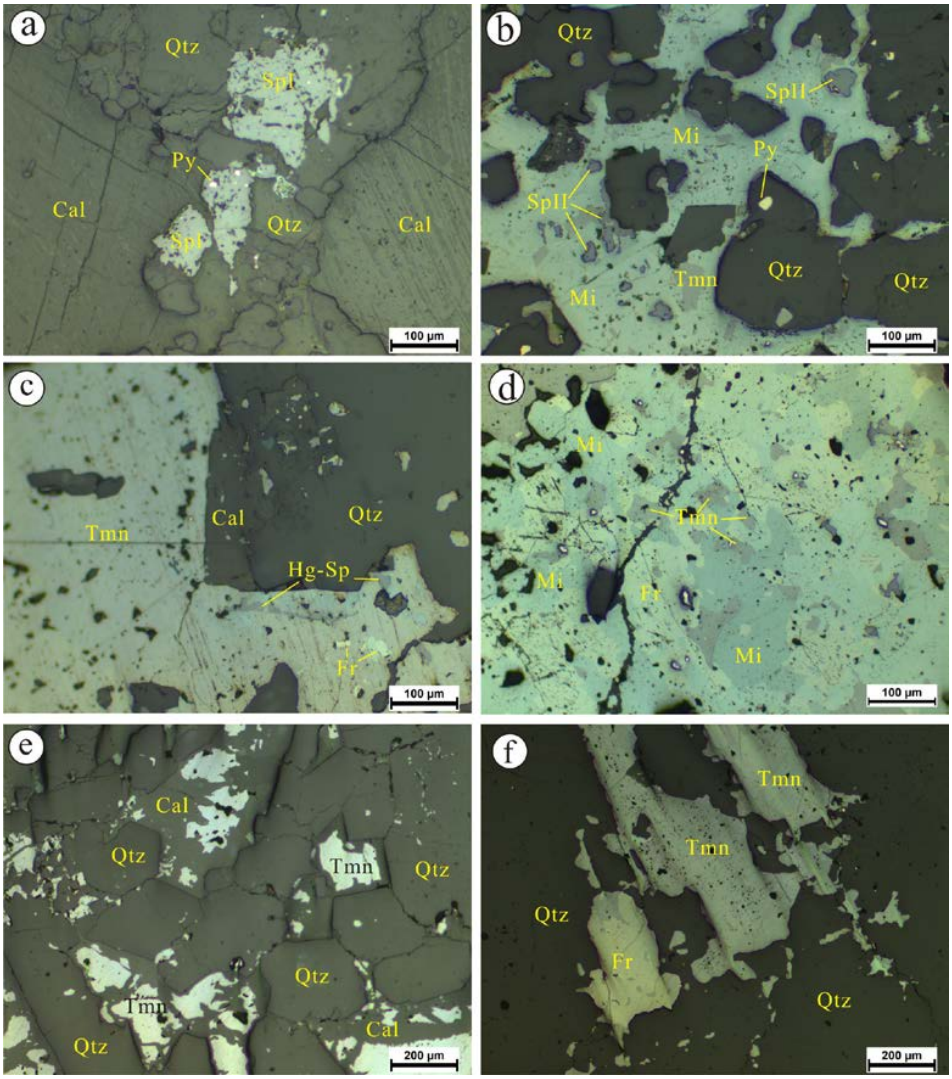

Figure 6. Photomicrographs of ore minerals and textures of the Dongping deposit: (**a**) sphalerite I (SpI) with pyrite (Py) hosted in quartz (Qtz); (**b**) sulfides corroding and filling the interstices in quartz, sphalerite II (SpII) forming island inclusions in miargyrite (Mi), with selenium metacinnabar also included by miargyrite; (**c**) sphalerite II as inclusions hosted in selenium metacinnabar; (**d**) complex sulfides aggregated with selenium metacinnabar replaced by Hg-bearing freibergite (Fr), and Hg-bearing freibergite replaced by miargyrite (Mi); (**e**) selenium metacinnabar preferentially replacing calcite (Cal) in quartz; and (**f**) irregular tiemannite and Hg-bearing freibergite in interstices in quartz.

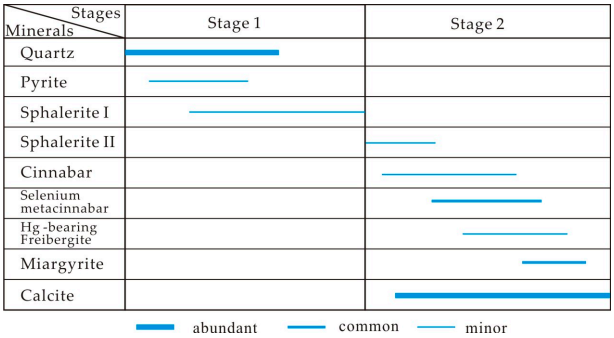

Figure 7. Paragenetic diagram of the Dongping Hg–Ag–Se deposit.

4.2. Chemical Composition of Hg-Bearing Sphalerite

The sphalerite II and sphalerite I from the Zn–Hg ores and Zn ores at the Chashula deposit, and the sphalerite II from the Hg–Ag–Se ores at Dongping deposit were analyzed by EPMA. The corresponding EPMA data are given in Table 1. Sphalerite II in the Chashula deposit contains 13.36–22.26 wt % Hg, 47.91–57.23 wt % Zn, 0.26–1.25 wt % Cd, and 0.00–0.10 wt % Fe. Meanwhile, sphalerite I contains 0.00–0.30 wt % Hg, 0.07–0.91 wt % Fe (with an abnormally high value of 2.28 wt %), and 0.42–1.44 wt % Cd in the Hg–Zn ores. Sphalerite I from the Zn zone contains 0.01–1.31 wt % Hg, 0.10–0.56 wt % Fe, and 0.15–0.90 wt % Cd. Sphalerite II of the Dongping deposit contains 10.12–14.67 wt % Hg, 54.10–56.77 wt % Zn, 0.00–0.09 wt % Cd, and 0.17–0.32 wt % Fe.

The Zn and Hg X-ray element-distribution maps show sphalerite II from the Hg–Zn ores at the Chashula deposit is homogeneous (Figure 8a–f), whereas sphalerite II from the Hg–Ag–Se ores at the Dongping deposit is inhomogeneous (Figure 8g–l).

Table 1. EPMA data for sphalerite II and I from the Chashula and Dongping deposits (wt %).

I.D.	Zn	Hg	Fe	Cd	Se	S	Total	I.D.	Zn	Hg	Fe	Cd	Se	S	Total
Sphalerite II in the Hg–Zn zone of the Chashula deposit								Sphalerite I in the Hg–Zn zone of the Chashula deposit							
1	51.27	19.04	0.05	0.74	0	29.4	100.5	9	66.05	0	0.29	1.44	0.02	33.21	101
2	51.5	19.27	0.05	0.97	0	28.99	100.78	10	64.68	0.08	0.91	1.01	0.02	32.4	99.09
3	51.01	18.83	0.03	0.89	0.01	29.29	100.05	11	66.87	0.3	0.07	0.9	0	32.58	100.73
4	53.73	16.81	0	0.39	0.02	29.82	100.76	12	64.95	0.06	0.88	1.24	0	32.79	99.92
5	51.27	19.89	0.01	0.74	0.01	29.62	101.54	13	65.91	0	0.81	0.85	0.04	32.4	100.02
6	50.24	19.03	0.02	0.34	0	29.07	98.69	Mean (n = 13)	65.69	0.06	0.57	0.95	0.01	32.82	100.1
7	49.53	19.47	0.04	0.28	0	29.37	98.69	Sphalerite I in the Zn zone of the Chashula deposit							
8	47.91	22.26	0.05	0.51	0	28.89	99.62	1	66.28	0.02	0.56	0.43	0.01	33.13	100.43
9	51.87	19.34	0.06	0.34	0	30.34	101.95	2	65.69	0.96	0.5	0.3	0	33.4	100.85
10	53.57	18.14	0.1	0.26	0.16	29.36	101.58	3	65.36	0.53	0.28	0.9	0	32.87	99.93
11	57.23	13.36	0	0.83	0.02	28.92	100.37	4	66.88	0.44	0.1	0.73	0.02	32.85	101.01
12	53.34	19.31	0.01	0.31	0	28.95	101.92	5	64.87	1.31	0.19	0.53	0	32.92	99.82
13	51.94	19.21	0	0.38	0	28.53	100.06	6	66.75	0.21	0.26	0.25	0	32.96	100.4
14	50.67	19.7	0.08	0.86	0.03	29.44	100.78	7	66.18	0.01	0.35	0.18	0	32.58	99.3
15	52.65	17.06	0.09	0.95	0	30.33	101.07	8	64.84	1.11	0.28	0.39	0	32.36	98.98
16	52.44	17.53	0.03	0.96	0	30.81	101.76	9	64.04	1.22	0.12	0.64	0.03	32.44	98.49
17	49.73	21.46	0.06	0.38	0	29.58	101.21	10	65.84	0.23	0.46	0.15	0.03	32.46	99.17
18	51.88	17.35	0.03	1.25	0.02	29.76	100.29	11	66.66	0.04	0.11	0.36	0	32.16	99.32
19	52.38	18.79	0.07	0.79	0	29.91	101.94	Mean (n = 11)	65.76	0.55	0.29	0.44	0.01	32.74	99.79
20	52.17	18.85	0	0.89	0	29.74	101.65	Sphalerite II in the Dongping deposit							
Mean (n = 20)	51.82	18.73	0.04	0.65	0.01	29.51	100.76	1	56.77	10.69	0.2	0.05	0.05	31.66	99.41
Sphalerite I in the Hg–Zn zone of the Chashula deposit								2	56.72	10.12	0.18	0	0.04	31.08	98.14
1	66.26	0.1	0.63	0.62	0	32.83	100.43	3	54.79	12.02	0.23	0.04	0.03	31.27	98.37
2	66.96	0	0.3	0.42	0.02	33.43	101.13	4	54.39	13.43	0.27	0.08	0.04	31.05	99.26
3	65.2	0.18	0.28	0.97	0	32.59	99.22	5	56.29	10.23	0.25	0	0.03	31.43	98.23
4	65.96	0.01	0.26	0.69	0	33.03	99.95	6	54.1	14.67	0.17	0.03	0.07	31.23	100.27
5	66.05	0	0.13	0.85	0	32.82	99.86	7	56.26	12.18	0.17	0.01	0.06	31.67	100.35
6	66.88	0	0.34	0.58	0	32.59	100.38	8	56.74	11.52	0.32	0.09	0.01	31.52	100.19
7	62.2	0	2.28	1.31	0	32.83	98.61	9	56.76	11.04	0.18	0	0.03	31.36	99.37
8	66.05	0	0.29	1.44	0.02	33.21	101.00	Mean (n = 9)	55.87	11.77	0.22	0.03	0.04	31.36	99.29

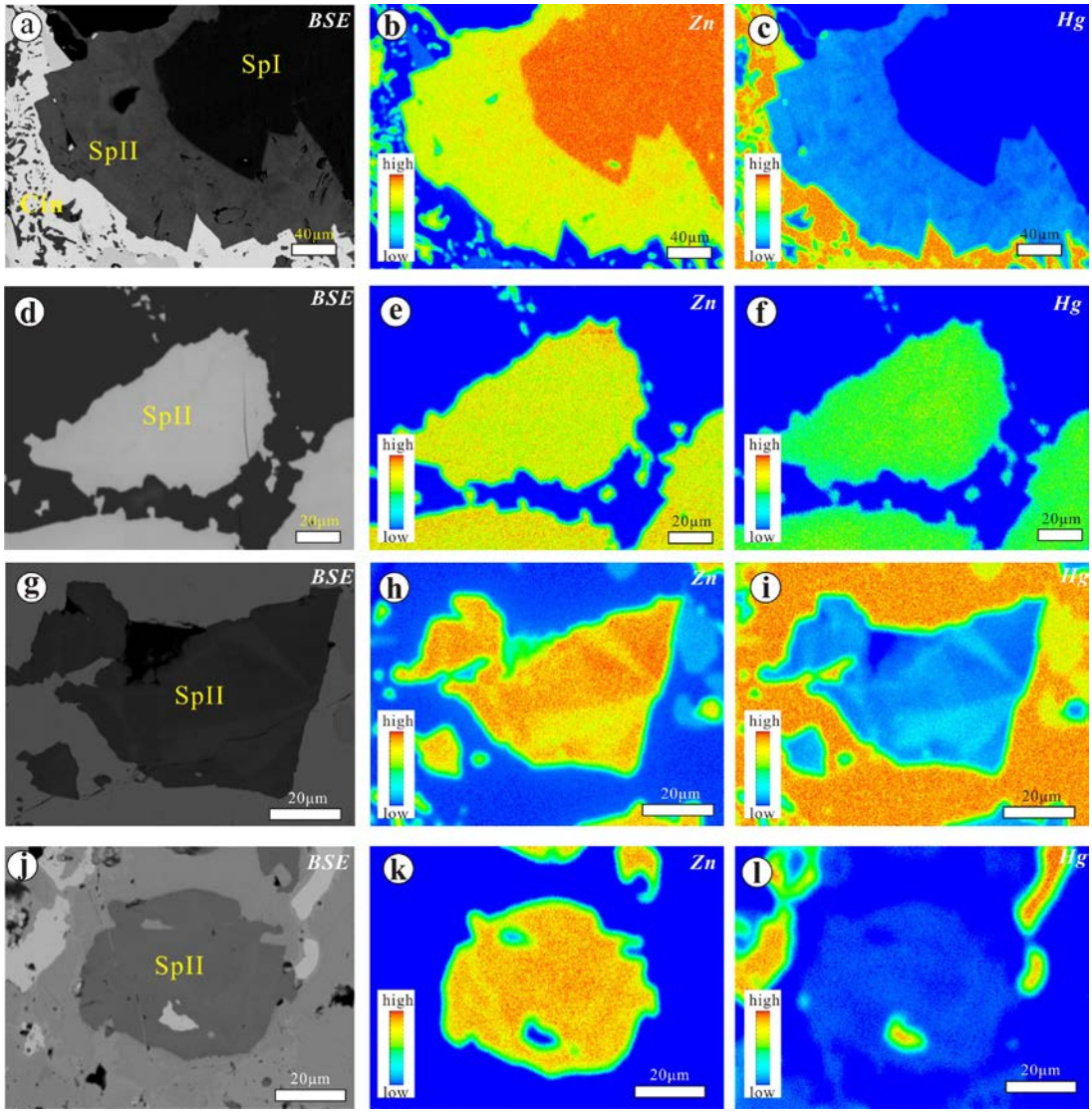

Figure 8. Backscattered electron images (**a**,**d**,**g**,**j**); and X-ray element-distribution maps for Zn (**b**,**e**,**h**,**k**); and Hg (**c**,**f**,**i**,**l**) of different occurrences of sphalerite II (SpII): (**a**–**f**) Zn and Hg maps of sphalerite II in Hg–Zn zones of the Chashula deposit, showing Hg–Zn distribution in minerals is homogeneous; and (**g**–**l**) Zn and Hg maps of sphalerite II in Hg–Ag zone of the Dongping deposit, showing Hg–Zn distribution in minerals is inhomogeneous.

4.3. Chemical Compositions of Zn-Bearing Cinnabar and Selenium Metacinnabar

The EPMA data of Zn-bearing cinnabar of the Chashula deposit and selenium metacinnabar of the Dongping deposit are given in Tables 2 and 3, respectively. The Zn-bearing cinnabar contains 5.13–7.05 wt % Zn, 73.16–79.21 wt % Hg, and 0.54–3.55 wt % Cd. The selenium metacinnabar contains 76.57–83.97 wt % Hg, 6.81–19.21 wt % Se, and 4.14–10.32 wt % S. The X-ray maps of these two minerals show that Zn and Hg are homogeneous in the Zn-bearing cinnabar (Figure 9), while Se and S are inhomogeneous in the selenium metacinnabar, with Se enriched in the core and S enriched in the rim (Figure 10).

Table 2. EPMA data for Zn-bearing cinnabar and cinnabar from the Chashula deposit (wt %).

Samples	Zn	Hg	Fe	Cd	Se	S	Total
Zn-bearing cinnabar							
4b2.1b	6.06	77.87	0.00	0.54	0.09	14.57	99.12
4b2.2	5.77	77.10	0.03	0.59	0.08	14.49	98.05
4b2.3	6.08	76.09	0.05	1.04	0.00	15.02	98.28
2kp3a4.1	6.72	75.18	0.00	3.09	0.15	15.00	100.14
2kp3a4.2	7.05	73.16	0.00	3.55	0.10	15.18	99.04
2kp3a4.3	6.64	74.65	0.00	3.50	0.07	15.12	99.97
4c1.7a	5.67	79.21	0.05	0.69	0.04	14.99	100.64
4c1.8a	5.13	78.98	0.00	0.61	0.07	14.88	99.66
Mean (n = 8)	6.14	76.53	0.02	1.70	0.07	14.91	99.36
Cinnabar							
2kp3a5.1	1.01	86.80	0.03	0.00	0.00	13.39	101.24
4c1.6c	0.03	86.45	0.00	0.02	0.12	13.33	99.94
zp2b1.1	0.00	85.10	0.00	0.00	0.03	13.55	98.67
zp2b1.2a	0.03	84.93	0.00	0.02	0.00	13.58	98.55
zp2a1.2b	0.03	86.52	0.03	0.00	0.00	13.91	100.48
zp2b1.3	0.00	85.23	0.00	0.00	0.02	13.71	98.96
Mean (n = 6)	0.18	85.84	0.01	0.01	0.03	13.58	99.64

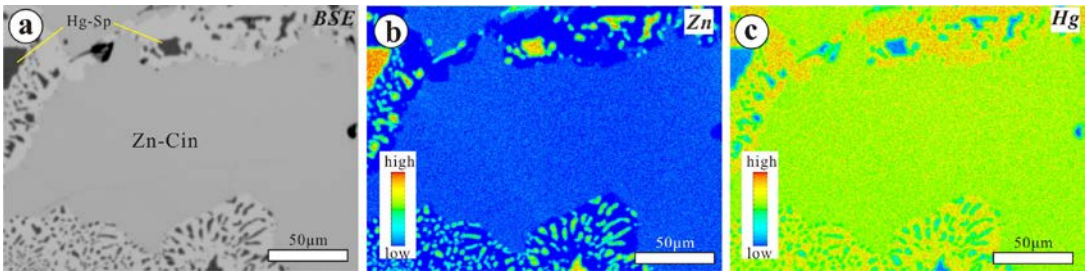

Figure 9. (**a**) Backscattered electron images; and (**b**,**c**) X-ray element-distribution maps for Zn and Hg, respectively, of Zn-bearing cinnabar (Zn-Cin) at the Chashula deposit.

Table 3. EPMA data for selenium metacinnabar from the Dongping deposit (wt %).

I.D.	Samples	Zn	Hg	Fe	Cd	Se	S	Total	I.D.	Samples	Zn	Hg	Fe	Cd	Se	S	Total
1	d7a1.1	0.00	79.73	0.00	0.00	13.91	6.64	100.28	16	d5a1.1	0.02	77.42	0.00	0.00	19.04	4.20	100.68
2	d7a1.5	0.13	80.10	0.02	0.01	13.24	7.13	100.62	17	d5a1.2	0.07	76.81	0.00	0.00	17.60	4.14	98.61
3	d7a1.6b	1.08	81.34	0.03	0.05	8.59	9.18	100.26	18	d5a1.3	0.17	80.18	0.02	0.00	14.63	6.44	101.45
4	d7a1.7a	0.59	83.97	0.00	0.01	6.81	10.32	101.71	19	d5a1.4	0.05	78.92	0.05	0.00	14.66	6.62	100.29
5	d7a1.8	0.22	77.20	0.02	0.00	19.21	4.34	100.99	20	d7b3.3	0.00	78.58	0.02	0.00	13.24	7.20	99.04
6	d7a1.9	0.00	81.13	0.00	0.00	11.07	8.01	100.21	21	d7b3.2	0.19	78.30	0.01	0.00	14.69	6.58	99.77
7	d7a1.10	0.61	80.75	0.06	0.04	10.30	8.33	100.09	22	d7b3.1	0.09	78.43	0.02	0.02	15.26	6.32	100.14
8	d7a1.11	0.25	79.65	0.01	0.00	13.18	6.89	99.97	23	d7b3.4	0.04	79.33	0.04	0.00	14.64	6.71	100.76
9	d7a1.14	0.26	79.65	0.04	0.06	11.22	7.98	99.21	24	d7b3.5	0.05	78.37	0.00	0.04	13.76	7.04	99.25
10	d7a1.16	0.08	77.76	0.02	0.00	13.95	6.58	98.38	25	d7b4.1	0.19	80.31	0.02	0.00	13.29	7.19	101.01
11	d7a1.17	0.23	80.95	0.03	0.03	10.40	8.69	100.32	26	d7b4.2	0.11	78.75	0.00	0.04	14.47	6.70	100.07
12	d7a1.19	0.60	81.00	0.06	0.02	8.91	9.34	99.94	27	d7b4.3	0.00	76.88	0.01	0.00	15.25	6.35	98.49
13	d7b1.1	0.03	76.57	0.01	0.00	18.39	4.65	99.65	28	d7b4.4	0.05	77.95	0.02	0.00	14.86	6.47	99.35
14	d7b1.2a	0.13	78.92	0.00	0.00	16.35	5.47	100.87	29	d7b4.5	0.13	79.38	0.03	0.00	13.54	7.16	100.23
15	d7b1.3	0.07	77.79	0.02	0.02	17.85	4.85	100.60	Mean (n = 29)		0.19	79.18	0.02	0.01	13.87	6.81	100.08

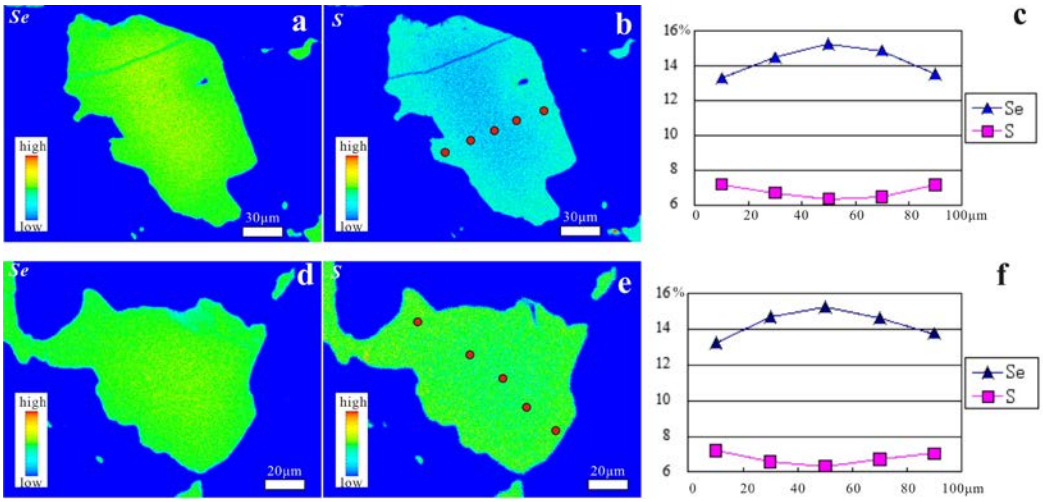

Figure 10. X-ray element-distribution maps for: Se (**a**,**d**); and S (**b**,**e**); and EPMA profiles of Se and S (**c**,**f**) from rim to core of typical selenium metacinnabar grains of the Dongping deposit.

4.4. XRD Data of Hg-Bearing Sphalerite and Metacinnabar

Sphalerite II and I from the Chashula and Dongping deposits were studied using XRD techniques. The XRD patterns of sphalerite II and I are shown in Figure 11, while the peak data are given in Table 4. All samples are cubic. Unit-cell parameter *a* increases with increasing Hg content.

Additionally, XRD data were also obtained for the cinnabar, Zn-bearing cinnabar and selenium metacinnabar. The cinnabar and Zn-bearing cinnabar are hexagonal varieties, with unit-cell parameters of $a = 4.148$ (0.001), $c = 9.488$ (0.002) Å for cinnabar and $a = 4.169$ (0.008), $c = 9.442$ (0.014) Å for Zn-bearing cinnabar, showing *a* increased, while *c* and density decreased with isomorphic substitution of Zn for Hg in Zn-bearing cinnabar. An XRD pattern of selenium metacinnabar is shown in Figure 12 and the peak data are given in Table 5. Selenium metacinnabar is cubic with unit-cell parameter $a = 5.940$ (0.001) Å. Compared with the ICDD references, parameter *a* of selenium metacinnabar from the Dongping deposit is closer to the metacinnabar (5.903 Å, PDF 22-729) than tiemannite (6.085 Å, PDF 8-469).

Table 4. XRD and crystallographic data for sphalerite II and I from the Chashula and Dongping deposits.

Samples	**Sphalerite II (Hg–Zn Aone in the Chashula Aeposit) ~20 wt % Hg**		**Sphalerite II (Hg–Ag–Se Orebody in the Dongping Deposit) ~10 wt % Hg**		**Sphalerite I (Zn Zone in the Chashula Aeposit) ~0.5 wt % Hg**		**Sphalerite I (Hg–Zn Aone in the Chashula Aeposit) ~0 wt % Hg**	
h k l	d_{eas}	I_{est}	d_{eas}	I_{est}	d_{eas}	I_{est}	d_{eas}	I_{est}
111	3.1552	100.0	3.1369	83.5	3.1320	100	3.1264	100.0
200	2.7317	4.2	2.7172	7.5	2.7062	1.0	2.7087	18.1
220	1.9293	21.6	1.9219	100.0	1.9118	9.6	1.9118	43.5
311	1.6461	30.5	1.6373	31.4	1.6322	6.9	1.6315	43.4
222	-	-	-	-	-	-	1.5612	2.7
400	-	-	-	-	1.3517	1.5	1.3626	1.7
331	-	-	-	-	1.2405	2.4	1.2498	2.2
a, Å	5.459 (0.001184)		5.432 (0.001149)		5.407 (0.000151)		5.409 (0.000684)	

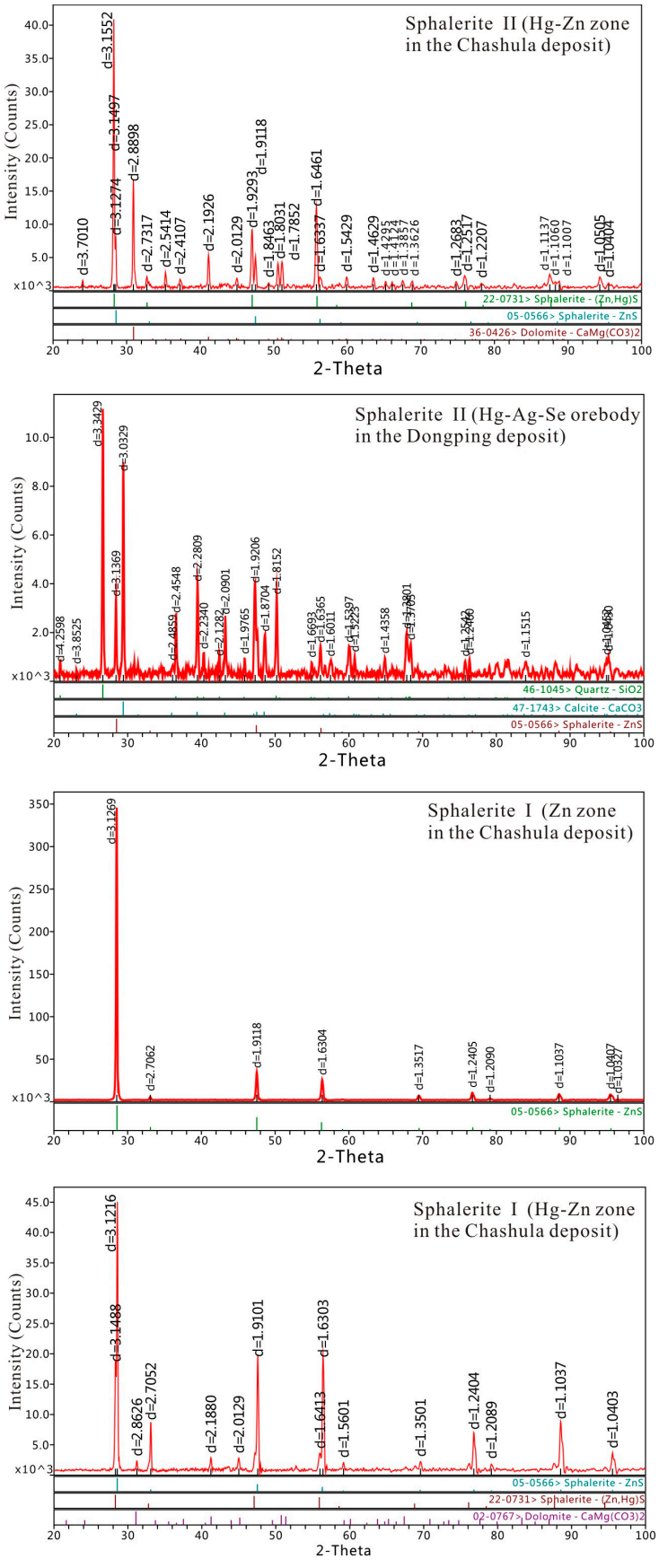

Figure 11. X-ray diffraction patterns of sphalerite II and I (peak data listed in Table 4) with ICDD references.

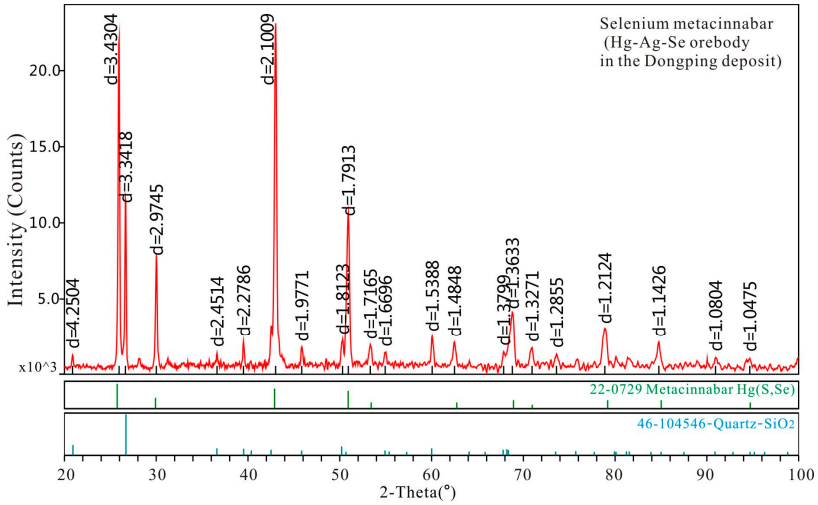

Figure 12. X-ray diffraction pattern of selenium metacinnabar (peak data listed in Table 5) with ICDD reference (No. 22-0729 metacinnabar).

Table 5. XRD and crystallographic data for selenium metacinnabar from the Dongping deposit, in comparison with ICDD data.

Samples	Tiemannite (PDF#08-0469, City Chemical Corporation, New York, USA)		Metacinnabar (PDF#22-0729, Gorkhon Aeposit, Russia)		Metacinnabar (Hg–Ag–Se ores in the Dongping Aeposit)	
h k l	*d*	*I*	*d*	*I*	d_{eas}	I_{est}
111	3.510	100.0	3.4100	100.0	3.4304	95.9
200	3.040	16.0	2.950	40.0	2.9745	33.4
220	2.151	50.0	2.090	80.0	2.1009	100.0
311	1.835	30.0	1.780	70.0	1.7913	44.2
331	1.396	10.0	1.355	30.0	1.3633	14.7
422	1.242	8.0	1.204	30.0	1.2124	11.2
511	1.170	4.0	1.136	30.0	1.1426	7.7
a, Å	6.085		5.903		5.940 (0.001)	

5. Discussion

5.1. Hg Contents of Sphalerite Reflect Spatial and Temporal Variations in the Carbonate-Hosted Hg Deposits

The minor and trace elements in sphalerite have application in identifying genetic ore types and the sphalerite temperature of formation [42,43]. Our EPMA data from the Chashula deposit show that the Hg contents of sphalerite I in the Hg–Zn ores (0.00–0.30 wt % Hg) are lower than in the outer Zn ores (0.01–1.31 wt % Hg), while the Hg contents of sphalerite II in the Hg–Zn zone are very Hg-rich (up to 22.26 wt % Hg). In hydrothermal systems, Hg is a high-vapor pressure element, and it does not readily enter the liquid phase at high temperature, forming and forms Hg-poor sphalerite. Fluid inclusion data of the Chashula deposit shows that the temperature reached up to 250 °C in the early stage [44]. Spatially, Hg contents of sphalerite I in the Hg–Zn zone are slightly lower than in the external Zn zone, probably because the temperature was higher in the central zone during Stage 1. With temperature decreasing, and the temperature of Stage 2 reaching 160–120 °C [44], Hg entered the fluid phase and formed Hg-rich ore fluid. In Stage 2, sphalerite II formed by replacing sphalerite I. The sphalerite II is intergrown with cinnabar, indicating Hg isomorphic substitution for Zn in sphalerite II reached saturation under the low-temperature conditions. The Hg contents of sphalerite II in the Chashula carbonate-hosted Hg deposit are higher than in the Eskay Creek volcanogenic massive sulfide deposit in Canada [11]. The Hg contents of sphalerite II in the Dongping deposit range from 10.12 to 14.67 wt %, lower than those of the Chashula deposit.

In the TFHB, Fe and Cd constitute minor elements within the ores. The Fe contents of sphalerite I and II in the Chashula and Dongping deposits are very low (below 1.00 wt %) and they belong to Fe-poor sphalerite. The Fe contents of sphalerite I in the Chashula deposit (avg: 0.57 and 0.29 wt % in the Hg–Zn and Zn zones, respectively, Table 1) are slightly higher than sphalerite II (0.00–0.10 and 0.17–0.32 wt % Fe in the Chashula and Dongping deposits, respectively). This indicates an inverse relationship between the Hg and Fe contents of sphalerite.

The Cd contents of sphalerite II and metacinnabar can reach high values in Hg-rich and complex ores (up to 15.80 wt %), depending on the temperatures of formation and Cd sources [10]. The EPMA data show that the Cd contents of sphalerite I (0.42–1.44 wt % Cd) and sphalerite II (0.26–1.25 wt % Cd) in the Chashula deposit are higher than sphalerite I (0.00–0.09 wt % Cd) in the Dongping deposit. Additionally, Cd contents of Zn-bearing cinnabar are up to 3.55 wt % Cd, while those of selenium metacinnabar are low (0.00–0.06 wt % Cd). Thus, the Hg and Cd contents in sphalerite do not show correlation.

Additionally, X-ray element-distribution maps of Hg and Zn in the sphalerite II and Zn-bearing cinnabar of the Chashula deposit are homogeneous (Figures 8b,c,e,f and 9), while those for the sphalerite II (Figure 8h,i,k,l) and selenium metacinnabar (Figure 10) of the Dongping deposit are inhomogeneous. The variation in mineral chemical compositions reflects that physiochemical conditions at the Chashula deposit were more stable than at the Dongping deposit, and they were suitable for Hg isomorphism.

5.2. Zn–Hg–S and Hg–Se–S Series Minerals

The Zn–Hg–S–Se component minerals form the ZnS (sphalerite)–HgS (metacinnabar) series and the HgS (metacinnabar)–HgSe (tiemannite) series [10]. Ores minerals of the Chashula and Dongping deposits, including sphalerite and cinnabar with Zn-bearing cinnabar, Hg-bearing sphalerite (sphalerite II), and selenium metacinnabar are plotted on a Zn–Hg–S–Se system diagram in Figure 13. The sphalerite, Hg-bearing sphalerite, Zn-bearing cinnabar, and cinnabar have a constant number of S atoms, but they do not form a continuous solid solution series because sphalerite has a cubic crystal structure, whereas cinnabar has an orthorhombic crystal structure. The Zn-bearing cinnabar is not stable, and it easily breaks down to Hg-bearing sphalerite and cinnabar (Figures 4g,h and 9) through the chemical reaction: (Hg,Zn)S → (Zn,Hg)S + HgS. In the Hg–Se–S series, Hg has a stable number of atoms and it shows continuous isomorphic substitution between Se and S, forming a wide range in selenium metacinnabar–tiemannite series.

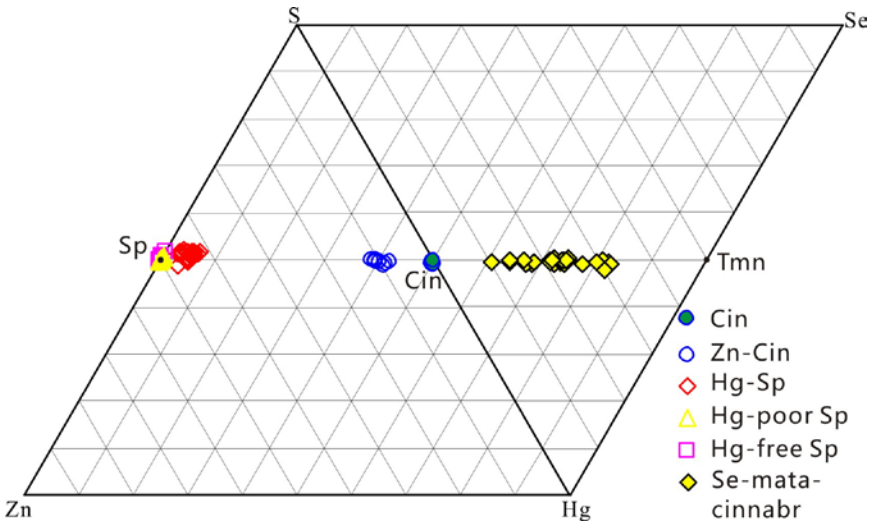

Figure 13. The Zn–Hg–S and Hg–Se–S series minerals of the Chashula and Dongping deposits.

5.3. Hg–Zn–Se Mineralization Style in the TFHB

Geological features of the Hg deposits in the TFHB are similar to the Mississippi Valley-type deposits [41], which are also hosted in carbonate rocks, with the metals derived from Hg–Se–Zn–Pb-enriched black shales of the Lower Cambrian [41,44,45]. In addition to Hg ores, the TFHB also contains Hg–Se, Hg–Zn, and Zn orebodies. For example, the Shangguangxi Hg–Se deposit of the Xinghuang orefield [46], Kezhai Hg–Se deposit in the Wanshan orefield [47], and Dongping Hg–Ag–Se deposit in the Shuiyingdong orefield [25,40] are reported in the TFHB. The Hg–Zn and Zn orebodies are distributed in the Chatian orefield [26–28,41]. Based on mineral studies of the Chashula Hg and Dongping Hg–Se–Ag deposits, dominant sphalerite was precipitated in Stage 1 of the mineralization process, while cinnabar and selenium metacinnabar or tiemannite precipitated in Stage 2. During Stage 2, cinnabar formed before the later selenium metacinnabar and silver minerals. Thus, Zn, Hg, and Se ores formed in different stages, and when the later mineralization was superimposed on the earlier, the compound Zn–Hg, Hg–Se ores were generated. The most important Se mineral is tiemannite. Selenide minerals are formed from oxidization and selenium-rich fluids [48]. The chemical composition of tiemannite varies due to the variation in physiochemical conditions during mineralization. The tiemannite contains 23.96–25.40 wt % Se in the Shangguangxi deposit [22,46], and selenium metacinnabar contains 6.81–19.21 wt % Se in the Dongping deposit. The characteristics of the ore fluids that formed the Hg–Se orebodies of the TFHB have not been determined. Thus, further fluid inclusion studies are needed to reveal the relationship between the Se contents of the metacinnabar-tiemannite series and the temperature of formation in the carbonate-hosted Hg deposits.

6. Conclusions

The mineral textures, assemblages, chemical compositions, and crystal structures of the Hg–Zn–Se–S minerals in the Chashula and Dongping carbonate-hosted Hg deposits of the TFHB were studied using microscopy, EPMA, and XRD, based on which we have drawn following conclusions.

(1) Microscopic observations of the mineralization of the Chashula and Dongping deposits show that the carbonate-hosted Hg deposits in the TFHB experienced two stages. Pyrite, sphalerite I (Hg-poor sphalerite), and quartz were formed in Stage 1, while Zn-bearing cinnabar, sphalerite II (Hg-bearing sphalerite), cinnabar, selenium metacinnabar, and Ag minerals were formed in Stage 2.

(2) The EPMA data show Hg contents of sphalerite I from the Chashula deposit contain low Hg (0.00–1.31 wt %), while sphalerite II is enriched in Hg (13.36–22.26 wt % Hg), which is the richest Hg in sphalerite within the TFHB. The sphalerite II of the Dongping deposit contains lower Hg (10.12–14.67 wt %) than that of Chashula deposit. The XRD data of sphalerite of the Chashula and Dongping deposits show that cubic unit cell parameter *a* gradually increases with increasing Hg content.

(3) The texture of the Zn-bearing cinnabar of the Chashula deposit shows that it is not stable, and that it easily breaks down to Hg-bearing sphalerite and cinnabar through the chemical reaction: (Hg,Zn)S $\rightarrow$ (Zn,Hg)S + HgS. The isomorphic substitution between Se and S in selenium metacinnabar of the Dongping deposit is continuous, forming a wide range of selenium metacinnabar compositions.

(4) The Zn, Hg–Zn, Hg, and Hg–Se mineralization styles in the deposits of the TFHB are the products of different stages in the mineralization process.

Acknowledgments: This work was jointly supported by the Innovation-driven Plan in Central South University (Grant 2015CX008), the National Natural Science Foundation of China (Grant 41302048), and the Open Fund of Key Laboratory of Mineralogy and Metallogeny, Chinese Academy of Sciences (Grant KLMM20110103).

Author Contributions: Jianping Liu and Shugeng Zhang conceived and designed the experiments; Jianping Liu and Yanan Rong performed the experiments; and Yanan Rong and Jianping Liu analyzed the data. All authors contributed to the preparation and writing of the manuscript.

Conflicts of Interest: The authors declare no conflict of interest.

References

1. Dill, H.G. The "chessboard" classification scheme of mineral deposits: Mineralogy and geology from aluminum to zirconium. *Earth Sci. Rev.* **2010**, *100*, 1–420. [CrossRef]
2. Rudnick, R.L.; Gao, S. Composition of the Continental Crust. In *Treatise on Geochemistry (Vol. 3 The Crust)*; Rudnick, R.L., Ed.; Elsevier: Amsterdam, The Netherlands, 2004; pp. 1–64.
3. George, M.W. *Mercury. U.S. Geological Survey, 2015 Minerals Yearbook*; USGS: Reston, VA, USA, 2016; pp. 102–103.
4. George, M.W. *Mercury. U.S. Geological Survey, Mineral Commodity Summaries*; USGS: Reston, VA, USA, 2017; pp. 108–109.
5. Yates, R.G.; Thompson, G.A. *Geology and Quicksilver Deposits of the Terlingua District, Texas*; U.S. Government Printing Office: Washington, DC, USA, 1959.
6. Zen, R. A preliminary observation on the regional distribution regularity and the main characteristics of mercury mineralizations in China. *Miner. Depos.* **1983**, *1*, 30–37. (In Chinese)
7. Song, S.H. *Mineral Deposits of China (Volume 1)*; Geological Publishing House: Beijing, China, 1989; pp. 414–446. (In Chinese)
8. Zou, Y.; Shi, D.; Zeng, L. China's mercury resource development and management countermeasures under the new situation. *China Min. Mag.* **2017**, *26*, 6–8. (In Chinese)
9. Hazen, R.M.; Golden, J.; Downs, R.T.; Hystad, G.; Grew, E.S.; Azzolini, D.; Sverjensky, D.A. Mercury (Hg) mineral evolution: A mineralogical record of supercontinent assembly, changing ocean geochemistry, and the emerging terrestrial biosphere. *Am. Mineral.* **2012**, *97*, 1013–1042. [CrossRef]
10. Vasil'ev, V.I. New data on the composition of metacinnabar and Hg-sphalerite with an isomorphous Cd admixture. *Russ. Geol. Geophys.* **2011**, *52*, 701–708. [CrossRef]
11. Grammatikopoulos, T.A.; Valeyev, O.; Roth, T. Compositional variation in Hg-bearing sphalerite from the polymetallic Eskay creek deposit, British Columbia, Canada. *Chem. Erde Geochem.* **2006**, *66*, 307–314. [CrossRef]
12. Radosavljević, S.C.; Stojanović, J.N.; Pačevski, A.M. Hg-bearing sphalerite from the Rujevac polymetallic ore deposit, Podrinje Metallogenic District, Serbia: Compositional variations and zoning. *Chem. Erde Geochem.* **2012**, *72*, 237–244. [CrossRef]
13. Jolly, J.L.; Heyl, A.V. *Mercury and Other Trace Elements in Sphalerite and Wallrocks from Central Kentucky, Tennessee and Appalachian Zinc Districts*; U.S. Geological Survey Bulletin; U.S. Government Printing Office: Washington, DC, USA, 1968.
14. Slim-Shimi, N.; Tlig, S. Mixed type sulfide deposits in Northern Tunisia, regenerated in relation to paleogeography and tectonism. *J. Afr. Earth Sci. Middle East* **1993**, *16*, 287–307. [CrossRef]
15. Jemmali, N.; Souissi, F.; Carranza, E.J.; Bouabdellah, M. Lead and sulfur isotope constraints on the genesis of the polymetallic mineralization at Oued Maden, Jebel Hallouf and Fedj Hassene carbonate-hosted Pb–Zn (As–Cu–Hg–Sb) deposits, Northern Tunisia. *J. Geochem. Explor.* **2013**, *132*, 6–14. [CrossRef]
16. Davidson, D.F. *Selenium in Some Epithermal Deposits of Antimony, Mercury and Silver and Gold*; U.S. Geological Survey Bulletin 1112-A; U.S. Government Printing Office: Washington, DC, USA, 1960.
17. Xinhuang Mercury Ming Company; No. 237 Metallurgical Geological Team of Hunan; No. 245 Metallurgical Geological Team of Hunan; Metallurgical Geology Institute of Hunan. Discovery of tiemannite and its prospecting significance. *Geol. Prospect.* **1975**, *1*, 35–37. (In Chinese)
18. Chen, D.; Sun, S. Coccinite in Shangguanxi, Hunan Province. *J. Changchun Univ. Earth Sci.* **1990**, *4*, 68. (In Chinese)
19. Chen, D.; Sun, S. Metacinnabar and tiemannite in Hunan-Guizhou (Xiangqian) mercury metallogenic belt. *Acta Petrol. Miner.* **1991**, *10*, 58–62. (In Chinese)
20. Huang, Z. Onofrite in the Dongping mercury deposit, Baojing, Hunan Province. *Acta Mineral. Sin.* **1991**, *1*, 274–277. (In Chinese)
21. Bao, J. Coccinite and its geological characteristics in the Jiudiantang mercury deposit. *Geol. Geochem.* **1982**, *9*, 56–57. (In Chinese)
22. Bao, Z. Geological characteristics and metallogenic effects of Xiangxi Hg–Pb–Zn deposit. *Geol. Prospect.* **1983**, *5*, 15–21. (In Chinese)

23. Liao, Z. Feature and genesis of zinc deposit in Dadongna mercury orefield. *Guizhou Geol.* **1999**, *16*, 315–320. (In Chinese)
24. Bao, Z.; Wan, R.; Bao, J. Geological feature of Shangguanqi-Gaozai Se–Hg deposit in Xinhuang of Hunan and significance of seeking for the deposit. *Guizhou Geol.* **1999**, *16*, 321–324. (In Chinese)
25. Xiang, P.; Niu, Y.; Feng, Q.; Ou, L.; Huang, X. Research on silver recovery of Doingping mercury-containing silver ore. *Met. Mine* **2005**, *34*, 407–410. (In Chinese)
26. Liu, A.; Zhang, M.; Chen, J.; Yang, T. Distribution Law of zinc ores at Dadongla mercury orefield, Tongren and predict for exploration. *Guizhou Geol.* **2007**, *24*, 188–192. (In Chinese)
27. Chen, J.; Liu, A.; Long, Q.; Xiong, W. The mineralization prospect analysis on the zinc ore in Yunchangping mercury mine field, Guizhou. *Guizhou Sci.* **2007**, *25*, 118–121. (In Chinese)
28. Yang, T.; Duan, Q.; Tian, W. Geological characteristics and prospecting potential of Chatian Pb–Zn–Hg deposit, Western Hunan Province. *Geol. Miner. Resour. South China* **2014**, *30*, 109–117. (In Chinese)
29. Wei, X.; Guo, Y.; Chen, Z. Hg-sphalerite and cell parameter formula. *Chin. Sci. Bull.* **1979**, *24*, 405–409. (In Chinese)
30. Zheng, P.; Liu, Z. Mineralogical features of mercury sphalerite from Chatian deposit, Fenghuang County. *Hunan Geol.* **1992**, *11*, 221–224. (In Chinese)
31. Bao, Z. Metallogenic mechanism of mercury-lead-zinc deposit in Western Hunan and Eastern Guizhou. *J. Guilin Coll. Geol.* **1987**, *7*, 159–170. (In Chinese)
32. Hua, Y. Preliminary study on the origin of mercury deposits in Guizhou and its vicinity. *Acta Geol. Sin.* **1981**, *2*, 139–148. (In Chinese)
33. Hua, Y.; Liu, Y. A genetic model for the Wanshan super-large mercury deposit, Guizhou. *Guizhou Geol.* **1996**, *2*, 161–165. (In Chinese)
34. Wang, H.; Hu, K.; Wu, G.; Chen, H.; Liu, C. Genesis of strata-bound mercury deposits in the border area between Hunan and Guizhou. In *Geology of Mercury Deposits of Guizhou Province, China*; Yan, J.P., Ed.; Geological Publish Hourse: Beijing, China, 1989; pp. 99–182. (In Chinese)
35. Wang, J.; Wen, H.; Shi, S. Characteristics and implications of REE, Carbon and oxygen isotopes of hydrothermal calcite from the mercury metallogenic belt in Hunan and Guizhou Provinces, China. *Acta Miner. Sin.* **2010**, *30*, 185–193. (In Chinese)
36. Lei, Y.; Dai, P.; Duan, Q.; Wang, G.; Zhao, W. Rotational shear tectonics and metallogeny of the mercury ore belt in Hunan and Guizhou Provinces, China. *Geotecton. Metallog.* **2012**, *36*, 525–529. (In Chinese)
37. Ye, L.; Cook, N.J.; Liu, T.; Ciobanu, C.L.; Gao, W.; Yang, Y. The Niujiaotang Cd-rich zinc deposit, Duyun, Guizhou Province, Southwest China: Ore genesis and mechanisms of cadmium concentration. *Miner. Depos.* **2012**, *47*, 683–700. [CrossRef]
38. Bao, J.; Wan, R.; Bao, Z. Discussion of the mercury mineralization related to the metallogenic belt of Hunan-Guizhou Province. *Beijing Geol.* **1999**, *2*, 5–12. (In Chinese)
39. Bao, Z. Mode of occurrence of two different types of orebodies in the Western Hunan-Eastern Guizhou mercury ore belt. *Miner. Depos.* **1985**, *4*, 81–88. (In Chinese)
40. Long, G.; Xie, S.; Peng, G. *Exploration Report of the Dongping Hg–Ag Deposit in Baojing County, Hunan Province*; No. 405 Geological Team Bureau of Geology and Mineral Resources of Hunan Province: Jishou, China, 1995; pp. 1–60. (In Chinese)
41. Yang, S.; Lao, K. Geological characteristics and ore indicators of lead-zinc deposits in northwestern Hunan, China. *Geol. Bull. China* **2007**, *26*, 899–908. (In Chinese)
42. Cook, N.J.; Ciobanu, C.L.; Pring, A.; Skinner, W.; Danyushevsky, L.; Shimizu, M.; Saini-Eidukat, B.; Melcher, F. Trace and minor elements in sphalerite: A LA-ICP-MS study. *Geochim. Cosmochim. Acta* **2009**, *73*, 4761–4791. [CrossRef]
43. Ye, L.; Cook, N.J.; Ciobanu, C.L.; Liu, Y.; Zhang, Q.; Liu, T.; Gao, W.; Yang, Y.; Danyushevskiy, L. Trace and minor elements in sphalerite from base metal deposits in South China: A LA-ICPMS study. *Ore Geol. Rev.* **2011**, *39*, 188–217. [CrossRef]
44. He, J.; Ma, D.; Liu, Y. The metallization geochemistry and hydrothermal concealed explosion model of the Chatian mercury deposit in Western Hunan. *J. Guilin Inst. Technol.* **1995**, *15*, 319–327. (In Chinese)
45. Schneider, J.; Boni, M.; Lapponi, F.; Bechstadt, T. Carbonate-hosted zinc-lead deposits in the lower Cambrian of Hunan, South China: A radiogenic (Pb, Sr) isotope study. *Econ. Geol.* **2002**, *97*, 1815–1827. [CrossRef]

46. Zheng, P. Mineralogical characteristics of tiemannite in Western Hunan. *Hunan Geol.* **1992**, *11*, 7–9. (In Chinese)
47. Hua, Y.; Cui, M. *Geology of the Wanshan Mercury Deposits in Guizhou*; Geological Publishing House: Beijing, China, 1995; pp. 1–143. (In Chinese)
48. Simon, G.; Kesler, S.E.; Essene, E.J. Phase relations among selenides, sulfides, tellurides, and oxides: II. Applications to selenide bearing ore deposits. *Econ. Geol.* **1997**, *92*, 468–484. [CrossRef]